Cerebral Cortex, August 2019; 3351–3362

doi: 10.1093/cercor/bhy204
Advance Access Publication Date: 28 August 2018
Original Article

ORIGINAL ARTICLE

Maturation of the Human Cerebral Cortex During Adolescence: Myelin or Dendritic Arbor?

Y. Patel[1,2], J. Shin[2,3], P.A. Gowland[4], Z. Pausova[3,5], T. Paus[2,6,7], and the IMAGEN consortium

[1]Institute of Medical Sciences, University of Toronto, Toronto, Ontario, Canada M5S 1A8, [2]Bloorview Research Institute, Holland Bloorview Kids Rehabilitation Hospital, Toronto, Ontario, Canada M4G 1R8, [3]The Hospital for Sick Children, University of Toronto, Toronto, Ontario, Canada M5G 1X8, [4]Sir Peter Mansfield Imaging Centre, School of Physics and Astronomy, University of Nottingham, Nottingham, NG7 2QX, UK, [5]Department of Physiology and Nutritional Sciences, University of Toronto, Toronto, Canada M5S 3E2, [6]Department of Psychiatry, University of Toronto, Toronto, Ontario, Canada M5T 1R8 and [7]Department of Psychology, University of Toronto, Toronto, Ontario, Canada M5S 3G3

Address correspondence to T. Paus. Email: tpaus@research.baycrest.org

Abstract

Previous in vivo studies revealed robust age-related variations in structural properties of the human cerebral cortex during adolescence. Neurobiology underlying these maturational phenomena is largely unknown. Here we employ a virtual-histology approach to gain insights into processes associated with inter-regional variations in cortical microstructure and its maturation, as indexed by magnetization transfer ratio (MTR). Inter-regional variations in MTR correlate with inter-regional variations in expression of genes specific to pyramidal cells (CA1) and ependymal cells; enrichment analyses indicate involvement of these genes in dendritic growth. On the other hand, inter-regional variations in the change of MTR during adolescence correlate with inter-regional profiles of oligodendrocyte-specific gene expression. Complemented by a quantitative hypothetical model of the contribution of surfaces associated with dendritic arbor (1631 m^2) and myelin (48 m^2), these findings suggest that MTR signals are driven mainly by macromolecules associated with dendritic arbor while maturational changes in the MTR signal are associated with myelination.

Key words: magnetic resonance imaging, magnetization transfer, membrane model, neurons, virtual histology

Introduction

Adolescence is a period of pronounced changes in physical, psychological, and social processes. A complex interplay between physiological (e.g., sex hormones) and experiential (e.g., peers, education) factors continues to shape the human brain during this developmental stage. Previous studies carried out with magnetic resonance imaging (MRI) in typically developing children and adolescents revealed robust age-related variations in various structural properties, such as changes in cortical thickness (Tamnes et al. 2017) and microstructure of white matter (Lebel and Beaulieu 2011). For the most part, however, neurobiology underlying these maturational changes in MRI-derived measures is unknown (Lerch et al. 2017). A handful of *post mortem* studies of the human cerebral cortex described age-related changes in the number of synaptic spines (Rakic et al. 1994; Huttenlocher and De Courten 1987; Petanjek et al. 2011) and the degree of myelination throughout the first 3 decades of life, including adolescence (Miller et al. 2012); in these studies, however, microscopic findings were not related to macroscopic measures such as cortical thickness. To provide a

bridge between MRI-derived metrics and the cellular composition of the human brain, we have developed a virtual-histology approach that relates inter-regional variations in MRI-derived metrics (e.g., cortical thinning) and variations in the expression of genes marking specific cell-types (e.g., pyramidal cells, oligodendrocytes) across the same cortical regions (Shin et al. 2017). The latter are derived from the Allen Human Brain Atlas (Hawrylycz et al. 2012), and verified for representativeness through a 2-step procedure (French and Paus 2015). Here we use this approach to ask whether inter-regional variations in magnetic transfer ratio (MTR), commonly assumed to index myelination (Schmierer et al. 2004), do indeed relate to myelination-related cell type (i.e., oligodendrocytes) or—alternatively—to other biological processes and cells.

Protons (hydrogen nuclei) can be classified into 2 distinct categories in biological settings—bound or free protons. Protons found in free water, such as intra/extracellular water, have relatively unrestricted movement and as such are termed the free pool of protons. Protons associated with macromolecules and cellular membranes (termed the bound pool of protons) are invisible in traditional MRI due to their short T_2 relaxation times (De Boer 1995; Henkelman et al. 2001; Tofts 2003). The presence of these macromolecules can be detected using a selective radiofrequency pulse that allows one to assess magnetization transfer (MT): the exchange of spin saturation between the bound pool of protons and the "free" pool of protons (associated with intra/extracellular water). The physical and chemical processes behind MT in a biological context are depicted in Figure 1. Predominantly, the exchange of spin saturation occurs through cross-relaxation (or exchange of spins) between a bound and free proton, and by chemical exchange of the proton. The exchange of energy is dependent on a variety of factors such as the amount of bound protons, macromolecular composition, and macromolecular surface chemistry (Grossman et al. 1994). Although a comprehensive biological basis of MT has yet to be investigated, we use the surface area of the interfaces between the bound (macromolecules) and free (water) pools (Fig. 1) as an indicator of efficient exchange of energy (Belton et al. 1988; Grossman et al. 1994; Koenig 1996; Luo 2009). A simple ratio (termed MT ratio—MTR) of the amount of signal loss due to spin exchange from the bound pool of protons can be calculated with a brain scan with (MT_{ON}) and without (MT_{OFF}) an MT saturation pulse by the following equation; $MTR = (MT_{OFF} - MT_{ON})/MT_{OFF}$ (Henkelman et al. 2001).

In biological systems, MTR is an indirect measure of macromolecular density, and it is sensitive to microstructural properties of tissues (Seiler et al. 2014). In white matter, MTR correlates with myelin content, as well as other structural properties (Filippi et al. 1998; Schmierer et al. 2004). It is assumed that myelin dominates MTR signals also in cortical (Mangeat et al. 2015; Whitaker et al. 2016) and subcortical (Fjær et al. 2013) gray-matter. Nonetheless, other macromolecules may represent less-appreciated sources of MT signal (Edzes and Samulski 1977; Henkelman et al. 1993).

Here we examine inter-regional variations in MTR values in the human cerebral cortex during adolescence, and use the

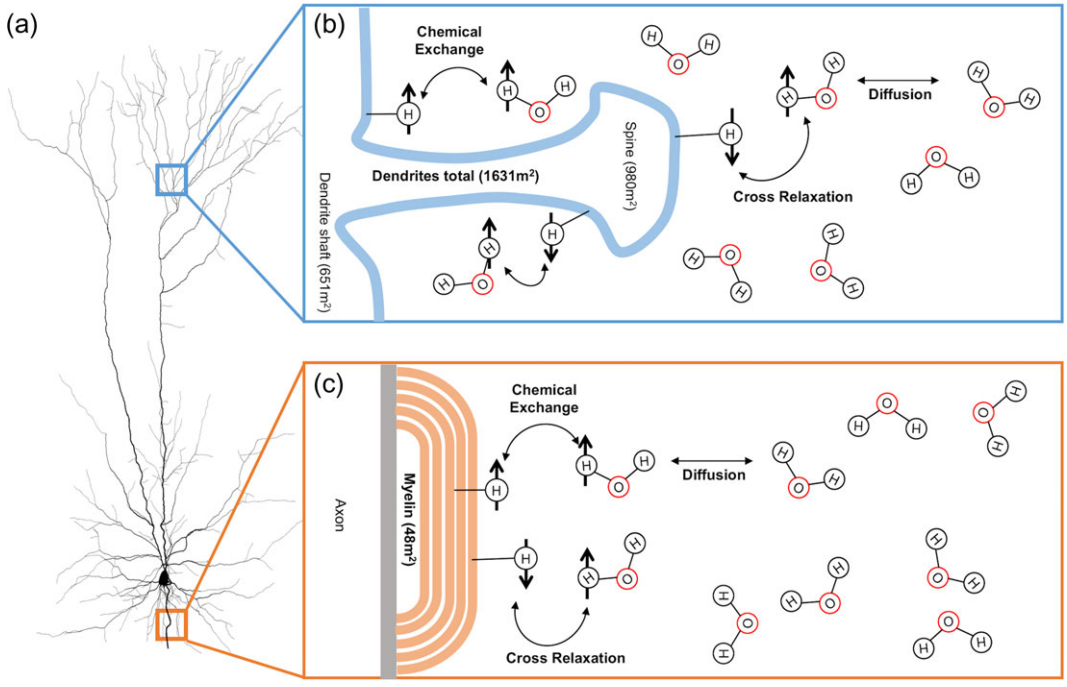

Figure 1. Processes behind magnetization transfer (MT) in a biological system (neurons). (*a*) Image of a cortical neuron (Cuntz et al. 2010) on the left; it has a disproportional amount of surface area associated with myelin sheaths (orange; 48 m^2) and dendrite (blue; 1631 m^2). (*b*) Microenvironment surrounding a dendritic spine exposed to the extracellular water. The bound pool of protons consists of hydrogen nuclei bound to semi-solid macromolecular structures whose molecular motion is low enough to facilitate MT, such as large macromolecules and cellular membranes (De Boer 1995; Henkelman et al. 2001; Tofts 2003). The free pool of protons consists of the hydrogen nuclei bound to unrestricted water molecules, such as intracellular/extracellular water (H_2O molecules above). Magnetization transfer occurs primarily through intermolecular dipole–dipole cross relaxation where there is exchange of spins between free and bound protons, and the chemical exchange of hydrogen nuclei (De Boer 1995; Henkelman et al. 2001; Tofts 2003). Numbers in brackets are the corresponding surface area as a result of dendrite shafts, and dendritic spines. (*c*) Microenvironment of an intracortical myelin sheath exposed to extracellular water. Number in brackets represents the estimated surface area of myelin exposed to the extracellular surface (not accounting of inner layers of myelin). See Results and Table 2 for derivation of estimated surface area of cellular compartments. Adapted from De Boer (1995).

above-described virtual-histology approach to identify their neurobiological substrate. We do so in a sample of typically developing adolescents, scanned twice, at 14 and 19 years of age. To facilitate interpretation of MTR signals in cerebral cortex, we also built a hypothetical model that quantifies the relative contribution of dendritic arbor and myelin, respectively, to the total surface area at the interface of the bound and free pools of protons.

Methods

Participants

A total of 281 healthy adolescents (mean age = 14.4 years, SD = 0.28 years; 148 males, 133 females) from the Nottingham cohort of the IMAGEN project were analyzed for Visit 1 of this study. Only participants from the Nottingham site were used as it was the only site to acquire MT-MRI scans. A total of 184 adolescents (mean age = 19.0 years, SD = 0.66 years; 94 males, 90 females) were included for Visit 2 analysis. For the longitudinal component, there were 150 adolescents (77 males, 73 females) who had both Visits 1 and 2 scans passing quality control. Participants with prior medical conditions such as mental-health disorders, tumors, or neurological disorders, were excluded. Further detail on recruitment, ethics, and standard operating procedures for the IMAGEN project (Schumann et al. 2010) are available at https://imagen-europe.com/standard-operating-procedures/.

MRI Acquisition

High-resolution structural MRI scans were acquired in both Visits using the same 3 T Philips Medical Systems scanner (Achieva). T1-weighted scans were acquired using a 3D gradient echo sequence (MPRAGE) adopted from the ADNI protocol (repetition time = 6.90 ms; echo time = 2.79 ms; flip angle = 9°; $256 \times 256 \times 137$ matrix, $1.1 \times 1.1 \times 1.1$ mm^3 voxel size). MT imaging was also acquired using the same 3 T scanner (FFE scan with MT saturation at +1 kHz, repetition time = 4.40 ms; echo time = 2.12 ms; flip angle 18°; $256 \times 256 \times 50$ matrix, $0.875 \times 0.875 \times 3$ mm^3 voxel size).

Image Processing Pipeline

T1-weighted scans were analyzed through the FreeSurfer (v6.0.0) (Dale et al. 1999) cortical reconstruction pipeline. MTR scans were calculated using "mincmath," and registered to T1-weighted scans using a 6 parameter boundary-based registration tool (bbregister) (Greve and Fischl 2009). At each cortical vertex, MTR values were extracted from the mid-point between pial surface and the gray-white matter boundary (i.e., at 50% distance between the cortical surface and the gray-white matter boundary). These values were averaged for all "mid-points" constituting each of the 34 regions of the Desikan-Killiany atlas (Desikan et al. 2006). Quality control was performed visually for image quality, cortical reconstruction, and image registration using the "ciftify" toolkit for QC page creation (found at https://github.com/edickie/ciftify) (Glasser et al. 2013).

Cell-Specific Gene Expression Analysis

To relate cell-specific gene expression profiles with MRI metrics (such as MTR), we use a previously described method that is visually represented in Supplementary Figure S1 (Shin et al. 2017). In brief, average gene-expression data from 6 donors (ages 24, 31, 39, 55, and 57 years) from the Allen Human Brain Atlas were mapped onto the 34 regions of the Desikan-Killiany atlas (French and Paus 2015). As implemented previously (Shin et al. 2017; Wong et al. 2017), the 20 737 genes whose expression levels were measured underwent a 2-stage filter for quality and consistency of data. In Stage 1, only genes with donor-to-median correlation in their inter-regional (34 regions) profiles greater than 0.446 were retained (8216/20 737 genes). In Stage 2, only genes with Allan-to-BrainSpan correlation in their inter-regional (11 regions) profiles greater than $r = 0.52$ were retained (2511/8216). The BrainSpan atlas (www.brainspan.org) provides an independent source of gene expression data in the human brain. Here, we used BrainSpan data from 9 donors: 5 males (ages 15, 18, 23, 36, and 37 years) and 4 females (ages 13, 21, 30, and 40 years). This 2-stage filter ensures that gene expression profiles are consistent across the 34 regions of the cerebral cortex across wider age range that includes adolescence and youth (13–23 years). Therefore, this set of 2511 genes is judged to be representative and, as such, suitable for the analyses reported here. Next, these genes were categorized according to data provided by Zeisel et al. (2015) as being specific to 1 of the 9 cell types present in the cortex, using single-cell RNA in mouse somatosensory (S1) cortex and the CA1 region of mouse hippocampus (Zeisel et al. 2015). Finally, a resampling based approach was used to test the association between inter-regional profiles of cell-specific gene expression and inter-regional profiles of MTR. The distribution of correlation coefficients for each cell-specific gene-expression profile and MTR profile is tested for significance with an empirical null distribution of correlation coefficients between random genes and MTR profile (repeated 10 000 times). The proportion of average correlation coefficients in the observed cell-specific distribution that exceed the null distribution correlation coefficients is then used to calculate a 2-sided false discovery fate adjusted P-value.

Sex Differences in Cell-Specific Gene Expression Analysis

To test whether the distributions of correlation coefficients (r) between ΔMTR-mRNA profiles for the S1 pyramidal genes differ between males and females, we carried out a 2-sided permutation test by randomly permuting the gender to get an empirical null distribution of the difference in average correlation coefficients of the male and female ΔMTR-profiles with the S1 pyramidal gene (with 1000 replications).

Statistical models

To analyze the effect of age on average cortical MTR and CT between Visits 1 and 2, we used a linear mixed-model analysis (n = 465) performed in JMP 13 statistical analysis software (Supplementary Fig. S4a,b). The mixed model used a restricted maximum likelihood approach, with age, sex, and age by sex interaction being fixed effects, while participant ID used as a random effect in order to account for the within-individual correlation of MTR measurements. A simple linear regression was used to test for significance (2-tailed P-values) between MTR and CT (between individuals and inter-regionally in each sex separately; Supplementary Fig. S5). Figures generated using JMP 13 software.

Gene Ontology Enrichment Analysis

A hypergeometric test was used to test enrichment of Gene Ontology (GO) groups with genes specific to CA1 pyramidal, ependymal, oligodendrocyte, and S1 pyramidal cells (each

tested separately, for a total of 4 analyses). The background gene-set included all 20 737 genes from the Allen Human Brain Atlas, and the foreground gene-set consisted of cell-specific genes. The analyses included all 3 domains (biological processes, cellular compartments, and molecular function) of GO groups containing between 10 and 100 genes. These GO groups were obtained using the GO.db and org.Hs.e.g.,db packages in R (Carlson 2016a, 2016b). The tests were carried out, using the "tmod" R package (Weiner and Domaszewska 2016). The P-values were corrected for multiple testing, using FDR-correction.

Data Availability

MTR and ΔMTR/year profiles for males and females across the 34 Desikan-Killiany regions are found at: https://figshare.com/s/84acf5a585c19127aae5 (used to generate Fig. 2*a*,*b*).

To recreate cell-specific gene expression ("virtual histology") analysis: https://figshare.com/articles/Cell-specific_gene-expression_profiles_and_cortical_thickness_in_the_human_brain/4752955/2 (used to generate Figs 3 and 4).

Results

Inter-regional Variation in Absolute MTR

High-resolution structural MRI (including MTR) was acquired in 281 adolescents (mean age of 14.4 years, Standard Deviation [SD] of 0.28 years; 55% males) at Visit 1 and 184 adolescents (mean age of 19.0 years, SD 0.66 years; 51% males) at Visit 2. Values of MTR were extracted from the cerebral cortex (mid-point between pial surface and gray-white boundary) via T1-weighted scans processed by the FreeSurfer (v6.0.0) cortical-parcellation pipeline (Dale et al. 1999). In order to assess the

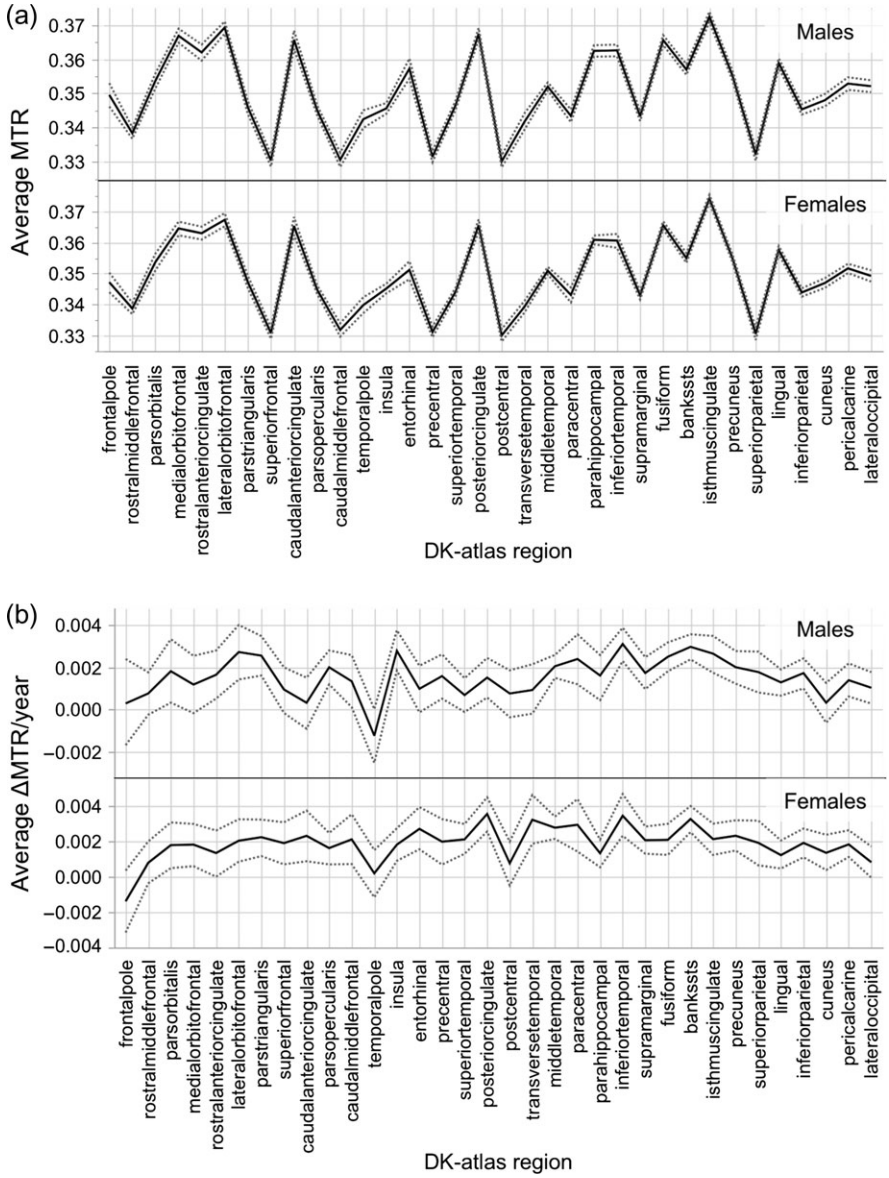

Figure 2. (*a*) Inter-regional variation in average magnetization transfer ratio (MTR) for males (top) and females (bottom) at Visit 1, across the 34 regions of the Desikan-Killiany atlas. (*b*) Inter-regional variation in average ΔMTR/year profiles for males (top) and females (bottom), across the 34 regions of the Desikan-Killiany atlas. Regions are arranged from anterior to posterior location (based on the center-of-gravity of each parcel). Dashed gray lines represent 95% bootstrapped confidence intervals.

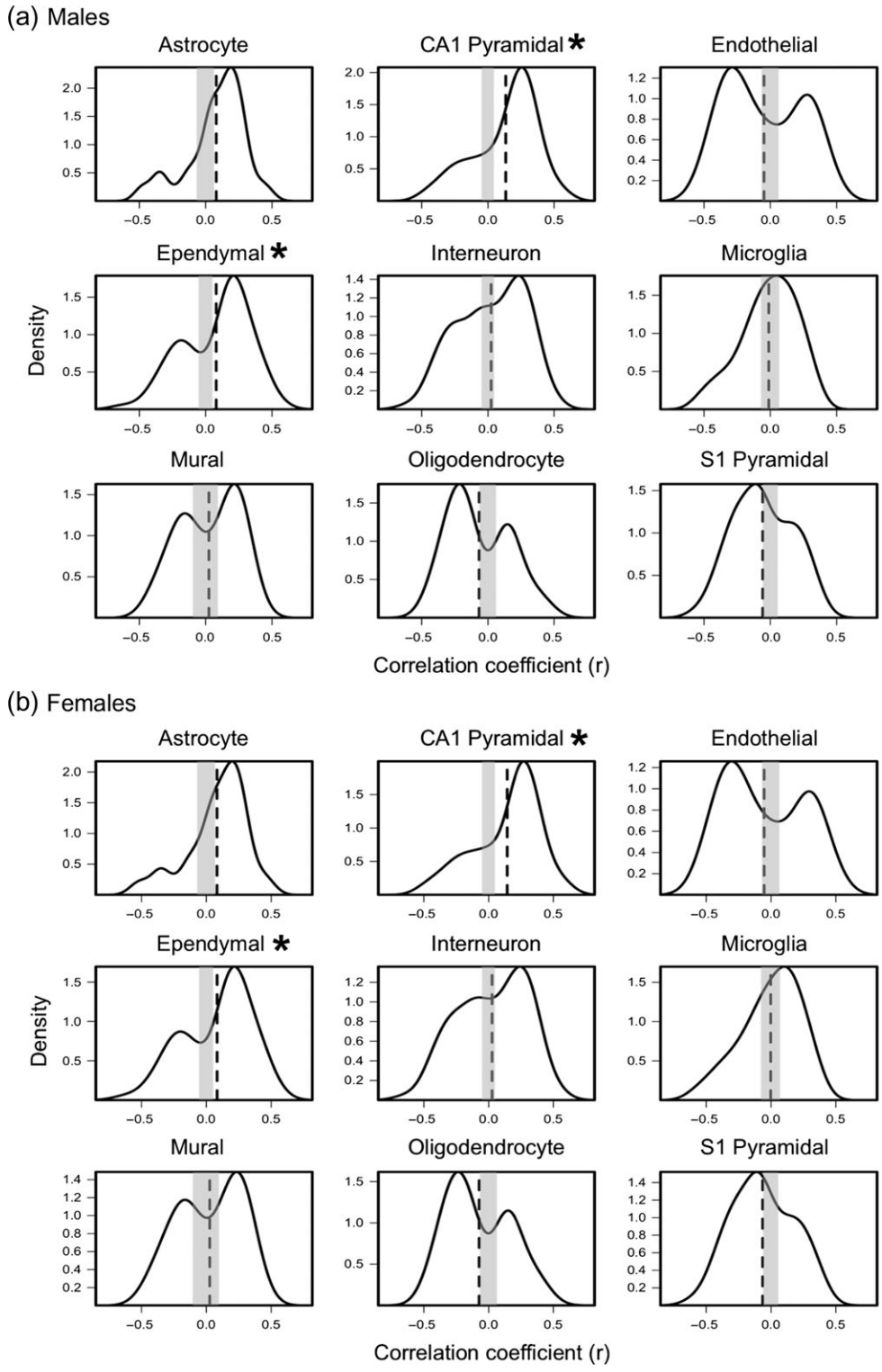

Figure 3. Distribution of correlation coefficients obtained by correlating (across the 34 regions) inter-regional profiles of expression of genes specific to 9 cell-types with inter-regional profiles of average MTR at Visit 1 in males (*a*) and females (*b*). Vertical dashed lines represents average expression-MTR correlation coefficient (quantified in Table 1). Gray box represents 0.5% and 97.5% of critical values obtained from the empirical null distribution of the average expression-MTR correlation coefficients. Red * indicates FDR-corrected *P*-value<0.05.

contribution of 9 cell types (Zeisel et al. 2015) (Fig. 2) to the inter-regional variations in absolute MTR values, we related inter-regional variations in cell-specific gene expression to inter-regional variations in MTR (Shin et al. 2017). MTR values were extracted from each of the 34 regions parcellated by FreeSurfer using the Desikan-Killiany atlas for each adolescent separately at Visits 1 and 2 (Fig. 2*a* and Supplementary Fig. S2). Inter-regional profiles of MTR at Visits 1 and 2 (group averages

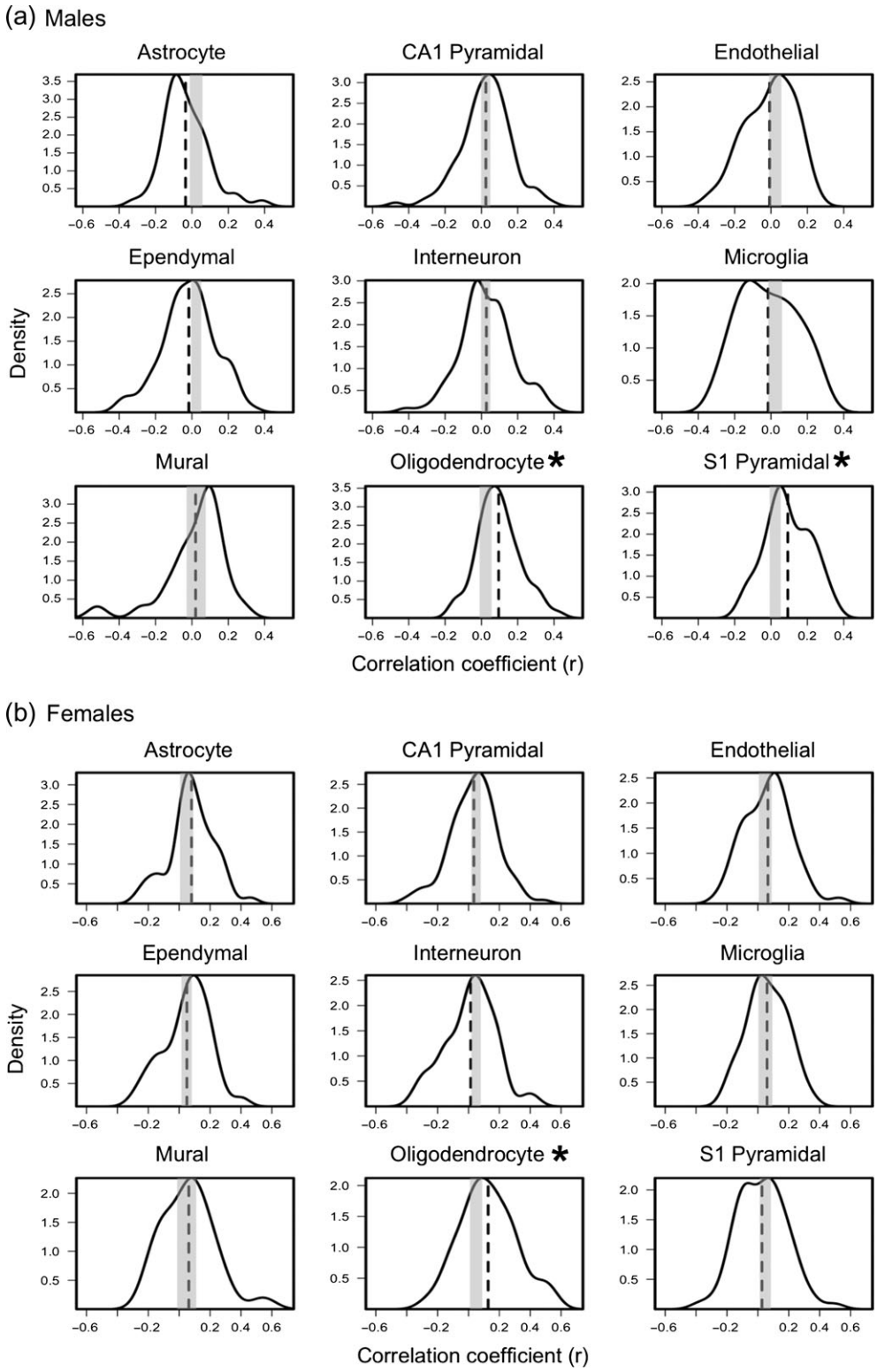

Figure 4. Distribution of correlation coefficients obtained by correlating (across the 34 regions) inter-regional profiles of expression of genes specific to 9 cell-types with inter-regional profiles of ΔMTR/year profile in males (*a*) and females (*b*). Vertical dashed-lines represents average expression-ΔMTR/year correlation coefficient (quantified in Table 1). Gray box represents 0.5% and 97.5% of critical values obtained from the empirical null distribution of the average expression-ΔMTR/year correlation coefficients. Red * indicates FDR-corrected *P*-value < 0.05.

for male and female adolescents, respectively) show associations with inter-regional profiles of expression of genes specific to CA1 pyramidal cells and ependymal cells (Fig. 3 and Supplementary Fig. S3). Table 1 shows the correlation coefficient between MTR and gene-expression profiles averaged over a given set of cell-specific genes, along with the associated false

Table 1 Average correlation coefficients between inter-regional profiles of cell-specific gene expression and inter-regional profiles of MTR

Cell (number of cell-specific genes)	Average r (FDR-corrected P-value)					
	MTR profiles				ΔMTR/year profiles	
	Male		Female		Male	Female
	Visit 1	Visit 2	Visit 1	Visit 2		
Astrocyte (54)	0.082 (0.06)	0.067 (0.07)	0.079 (0.05)	0.070 (0.06)	−0.035 (0.75)	0.08 (0.32)
CA1 pyramidal (103)	**0.143 (0.00089)***	**0.131 (0.00089)***	**0.134 (0.00089)***	**0.119 (0.00089)***	0.024 (0.75)	0.034 (0.99)
Endothelial (57)	−0.053 (0.18)	−0.046 (0.26)	−0.048 (0.22)	−0.022 (0.56)	−0.007 (0.86)	0.065 (0.59)
Ependymal (84)	**0.083 (0.01035)***	**0.072 (0.01259)***	**0.079 (0.01395)***	**0.078 (0.00539)***	−0.017 (0.75)	0.05 (0.69)
Interneuron (100)	0.026 (0.41)	0.027 (0.33)	0.024 (0.42)	0.024 (0.53)	0.027 (0.75)	0.014 (0.98)
Microglia (48)	−0.003 (0.94)	0.00 (0.99)	−0.012 (0.73)	−0.002 (0.96)	−0.016 (0.75)	0.059 (0.58)
Mural (25)	0.026 (0.69)	0.030 (0.55)	0.025 (0.69)	0.039 (0.52)	0.02 (0.75)	0.062 (0.58)
Oligodendrocyte (60)	−0.073 (0.06)	−0.032 (0.34)	−0.066 (0.09)	−0.014 (0.71)	**0.095 (0.00045)***	**0.127 (0.00269)***
S1 pyramidal (73)	−0.064 (0.06)	−0.033 (0.34)	−0.057 (0.09)	−0.034 (0.46)	**0.093 (0.00045)***	0.027 (0.99)

Average correlation coefficients obtained by correlating (across the 34 regions) inter-regional profiles of expression of genes specific to 9 cell-types with inter-regional profiles of average MTR at Visits 1 and 2, and with inter-regional profiles of ΔMTR/year in both sexes. False-discovery rate (FDR) corrected P-values are in brackets. *FDR-adjusted P-value < 0.05.

Table 2 Total surface area as a result of different neuronal cellular compartments in the average neocortex

Cellular compartment	Total length (m)	Average diameter (μm)	Surface area (m^2)
Dendrite shafts	211 427 054	~1	651
Dendritic spines	342 900 000	~0.25	980
Myelinated axon	20 049 000	~0.76	48
Dendrites total			1 631

Estimates of total length, average diameter, and surface area associated with dendrite shafts/spines, and myelinated axon derived from theoretical model of membranes in the average cerebral cortex. See Supplementary Calculations for further details.

discovery rate (FDR) adjusted P-values for each cell type at Visit 1 and 2. None of the other cell types were associated with the inter-regional MTR profiles in these analyses. To determine biological processes related to the cell-specific genes, we perform a GO analysis to assess enrichment of GO groups. CA1 pyramidal and ependymal cell-specific genes were enriched significantly for biological processes related to dendritic branching and cilia, respectively (Supplementary Table S1). The top 2 GO terms for CA1 pyramidal gene-set were "positive regulation of dendrite extension and regulation of dendrite extension" and, for ependymal specific gene-set, "cilium movement and epithelial cilium movement."

Inter-regional Variation in ΔMTR/Year

Using the longitudinal subset of data (n = 150, 51% males), we calculated the change (per year) in MTR in each of the 34 regions of the cerebral cortex (Fig. 2*b*). Inter-regional profiles in ΔMTR/year show associations with gene-expression profiles specific to oligodendrocytes and S1 pyramidal cells, the latter in males only (Fig. 4 and Table 1). Using a 2-sided permutation test, we cannot reject the null hypothesis (P = 0.23) regarding sex differences between males and females in the distribution of correlation coefficients (r) between ΔMTR/year profile and S1 pyramidal specific gene set. GO analysis of oligodendrocyte and S1 pyramidal specific genes identify myelination and potassium channel activity, respectively, as important biological processes in these cell-type specific gene sets (Supplementary Table S2). Although oligodendrocyte specific genes were not enriched significantly in this GO analysis, the top 2 GO terms were "paranode/juxtaparanode region of axon." S1 pyramidal specific genes were enriched significantly for "voltage-gated potassium channel activity/complex."

Hypothetical Model of Membranes: Dendritic Arbor Versus Myelin

The exchange of energy in MT phenomena is related to the surface area of the interfaces between the bound (macromolecules) and free (water) pools (Belton et al. 1988; Grossman et al. 1994; Koenig 1996; Luo 2009). To complement findings from virtual histology, we attempt to model the amount of surface area contributed by dendritic arbor or myelin within the cortex (Table 2). This hypothetical model is based on existing histological literature on the morphology of human neocortical neurons. Although this model cannot account for the areal and laminar heterogeneity in cellular morphology (due to limited availability of data), we have utilized the most accurate morphological numbers obtained with state-of-the-art methodologies such as intracellular dye staining, and 3D neuron reconstruction.

The human cerebral cortex contains roughly 21.05 billion neurons, as quantified in a sample of 94 brains ranging from 18 to 93 years of age (Pakkenberg and Gundersen 1997). This number compares well with the more recent estimate of 16.3 billion neurons obtained in a smaller sample (n = 4) (Azevedo et al. 2009). It has been estimated that 75% of these neurons are excitatory pyramidal neurons, and 25% inhibitory interneurons (DeFelipe and Fariñas 1992; Markram et al. 2004). Total dendritic length of pyramidal neurons (reconstructed in 3D space) across different layers of the temporal cortex vary from 14 679

μm in layer II/ layer III to 9193 μm in layer V/ layer VI (Mohan et al. 2015). A weighted average was used to account for the diverse distribution of neurons within each layer of the cortex quantified via a cortical minicolumn (DeFelipe 2011). We estimate that in the average human cerebral cortex, dendrite shafts contribute to 651 m^2 of interface surface area, with a total length of 211 427 054 m (Supplementary Calculations).

Dendrites have spiny processes protruding from the shaft, thus increasing receptive area and facilitating cell-to-cell communication via synapses (DeFelipe and Fariñas 1992). These dendritic spines are highly variable in size, morphology and density across cortical regions and layers (DeFelipe and Fariñas 1992). Spine density varies from 1 to 3 spines per μm of dendrite shaft across cerebral lobes (occipital to frontal, respectively) (Elston et al. 2001). We used a cylinder to model the spine shaft with a length of 1.35 μm and diameter of 0.25 μm; we modeled the spine head as a compartment with a surface area of 2.80 $μm^2$ (Benavides-Piccione et al. 2002; Eyal et al. 2016). From our estimates, there are roughly 254 billion spines contributing to 980 m^2 of membrane area in the human cerebral cortex; this is based on a conservative estimate of 1.5 spine per 1 μm of dendrite, and assuming that 1 out of 5 neurons lack spines (Supplementary Calculations) (DeFelipe and Fariñas 1992; Benavides-Piccione et al. 2012). Altogether, we estimate that dendrites (shafts) and their spines represent a total surface area of 1 631 m^2 in the average human cerebral cortex (Table 2).

To quantify myelin-related surface area in the human cerebral cortex, we focused exclusively on the exterior surface of myelin sheaths—where there is greatest opportunity for cross relaxation and subsequent diffusion of saturated protons (Fig. 1). In a limited number of human brains, myelination has been quantified using stereological methods across a number of cortical regions including frontopolar, visual, somatosensory, and motor cortices (Miller et al. 2012). On average, there is 0.041 μm of myelinated fiber in 1 $μm^3$ of volume in the cortex, as quantified in 3 individuals (ages 16, 20, and 23 years) (Miller et al. 2012). Myelinated fibers found in the cerebral cortex vary greatly in diameter (from 0.16 to 9 μm), with a majority of fibers averaging below 1 μm in their diameter (Liewald et al. 2014). The exterior surface area of myelin (in contact with extracellular water) is roughly 48 m^2, using a total length of 20 049 000 m of myelinated axons, and an average fiber diameter of 0.76 μm (Innocenti et al. 2013) (Table 2 and Supplementary Calculations). For completeness, we also calculate the total axonal length (myelinated and unmyelinated together; 336 800 000 m) and their total surface area (317 m^2) in the human cerebral cortex.

Inter-regional Versus Global MTR

To allow comparison with a previously reported cross-sectional study (Whitaker et al. 2016), we tested the effect of age on average global (across the entire left cerebral cortex) MTR (Supplementary Fig. S4a). Using a linear mixed model with random effects analysis, we report an increase in average global MTR with age ($P < 0.0001$), and decreases in global CT (left hemisphere) with age ($P < 0.0001$) (Supplementary Fig. S4a,b). At Visit 1, global CT correlated negatively with global MTR in males only ($P = 0.0008$; Supplementary Fig. S5a); no such correlations were observed at Visit 2 in either sex group. Regional MTR did not correlate with regional CT in Visit 1 or 2 in both sexes (Supplementary Fig. S5b). Finally, we did not observe any correlations between global ΔMTR/year and global ΔCT/year in both sexes (Supplementary Fig. S5c). We did observe a negative correlation ($P = 0.02$) between regional ΔMTR/year and regional ΔCT/year in males only (but sex difference between correlations was not significant, $P = 0.06$) (Supplementary Fig. S5d).

Discussion

Here we report clear differences in the biological processes associated with inter-regional variations in absolute values of MTR (at one time point) versus inter-regional variations in ΔMTR/year. We also provide confirmation of age-related increase in average MTR (Whitaker et al. 2016) in the cerebral cortex during human adolescence using longitudinal data (Supplementary Fig. S4a).

Absolute Values of MTR and Dendritic Arbor

Across the cerebral cortex (34 regions), absolute values of MTR correlate with gene-expression profiles specific to CA1 pyramidal cells and ependymal cells (both sexes, both visits). This is not the case for oligodendrocyte-specific gene expression, suggesting that absolute values of MTR are not sensitive to intracortical myelination. GO groups related to dendrites and dendritic branching are enriched significantly in the CA1 pyramidal gene-set (Supplementary Table S1). Dendrites (and their spines) contribute up to 90–95% of the total surface area of a cortical neuron (Ulfhake and Kellerth 1981). Variations in dendritic branching may drive variations in absolute MTR values as higher surface-area of cellular membranes relates to greater energy transfer between the 2 pools of protons (Koenig 1996; Luo 2009). Additionally, lipids bilayers are effective macromolecular structures for MT between the bound and free pool of protons (De Boer 1995). Using our quantitative hypothetical model of neuronal membranes, compared with myelin—dendrites (and their spines) contribute 34-fold (1631 m^2/48 m^2) more surface area exposed to the extracellular water, further indicating that MTR at a single time-point is more sensitive to cellular membranes associated with dendrites rather than myelin.

Ependymal cell-specific genes were also correlated with inter-regional profiles of absolute MTR. The ependymal gene set ($n = 84$ genes) was enriched significantly for the biological processes pertaining to axoneme assembly and cilium movement, as well as for the cellular compartments pertaining to axoneme and ciliary plasm. These genes appear to be associated not only with motile cilia, found on the surface of ependymal cells, but also with the primary nonmotile cilia found on every cortical neuron (Lee and Gleeson 2010); the 2 types of cilia may share up to 75% common proteins (Ishikawa et al. 2012). The GO term "axoneme" (GO:0005930) refers to the inner microtubule-based cytoskeletal core found in cellular "appendages" such as cilia (including the core of primary cilia) (Pazour and Witman 2003). Given this, it is likely that the correlation between the inter-regional variation of ependymal-specific genes and inter-regional MTR profiles is related to primary cilia found in every neuron, rather than ciliary movement or ependymal cells specifically. A primary cilium is a single microtubule-based appendage that extends from the surface of a cell. Primary cilia serve as a cellular "antenna," and are involved in several neuronal processes such as cell-polarity axonal guidance (Lee and Gleeson 2010). Disruption of ciliary function in cortical neurons is followed with abnormal neuronal morphology and impaired dendrite outgrowth (Guadiana et al. 2013). Restoration of cilia function recovers normal dendrite outgrowth, suggesting an

important role of primary cilia in maintaining dendritic branching (Guadiana et al. 2013). We speculate that the ependymal-specific correlation with inter-regional variation in absolute MTR is related to primary cilia-related genes, and consequently, dendritic arborization.

ΔMTR/Year and Myelination

The association between inter-regional profiles of ΔMTR/year and oligodendrocyte-specific gene expression supports a myelin-based interpretation of this developmental process. Oligodendrocyte-specific gene set was not enriched significantly (after FDR-corrections) with myelin-related cellular compartments. Nonetheless, the top 2 GO terms (paranode/juxtanode region of axon) are cellular compartments enclosed in layers of myelin (Trapp and Kidd 2004). Additionally, phosphatidylinositol-related molecular factors were also among the top 10 GO terms (Supplementary Table S2). Alongside the diverse roles of phosphatidylinositol bisphosphate as a secondary messenger, it is also required for stable membrane binding of myelin basic protein, and consequently involved in myelin maintenance (Nawaz et al. 2009). Although this GO analysis was not significant, oligodendrocytes have a unique function (i.e., myelination/myelin maintenance) compared with other glia cells (Gibson et al. 2014). Therefore, we interpret oligodendrocyte-specific signal as related to intracortical myelination. Post mortem histological studies support the observation of continued myelination during adolescence, well into the third decade of life (Benes et al. 1994; Miller et al. 2012). We speculate that, in the analyses of absolute MTR values, this oligodendrocyte-related (myelin) signal is masked by other sources of macromolecular/bound protons, namely extensive membrane surfaces of the dendritic arbor. The signal is revealed only after "subtracting" these dominant (dendrite-related) signals through longitudinal analysis (i.e., ΔMTR).

In males, we observed an association between ΔMTR profile and S1 pyramidal specific expression. As this gene set is enriched for neural-activity related mechanisms, we suggest that it is consistent with neural activity-dependent oligodendrocyte activation (Jensen and Yong 2016). Oligo-activity and myelination are stimulated by neural activity (Jensen and Yong 2016), and—in this manner—may influence the observed increase in MTR during cortical maturation. Stimulation of the mouse M2 motor cortex increased number of progenitor/mature oligodendrocytes and increased myelin thickness (Gibson et al. 2014). Experience-dependent myelination, thought to be a result of experience-related neural activity, has also been observed; dark-reared mice have reduced number of myelinated axons in the optic nerve compared with control (Gyllensten and Malmfors 1963). Taken together, it is possible that experience-driven activity-dependent myelination during human adolescence may explain the inter-regional variation in change in MTR per year.

Hypothetical Model of Membranes

Our model of membranes attempts to quantify the relative contributions of dendrites and myelin to MT signals. It is important to state that the cerebral cortex is highly heterogeneous in nature in terms of spine density (Elston et al. 2001), neuronal morphology (DeFelipe and Fariñas 1992), and degree of myelination (Miller et al. 2012). At the same time, we are limited by the availability of data from different cortical regions, and as such this model serves only as the first approximation with regards to which cellular compartments dominate within the human cerebral cortex. This model also does not take into account the effect of age on dendritic spines and neuronal morphology. It is known that dendritic-spine density diminishes gradually between 9 and 22 years of age (Petanjek et al. 2011). Furthermore, certain morphological measures of dendritic length (Bianchi et al. 2012), and dendritic-spine density (Petanjek et al. 2011; Bianchi et al. 2013) were not included due to methodological considerations. For example, the use of rapid Golgi stain "for spine number and dendritic length are likely to be an underestimation of the actual biological values" as a result of constraints in traditional light microscopy (Bianchi et al. 2013; Sala and Segal 2014). For this reason, we used data from 3D spine reconstruction (Benavides-Piccione et al. 2012) rather than from Golgi stained microscopy (Petanjek et al. 2011; Bianchi et al. 2013). Due to heterogeneity in dendritic-spine density across regions of the cortex (ranging from 0.2 to 3.5 spines per 1 μm of dendrite), we used a highly conservative estimate of 1.5 spines per 1 μm of dendrite to model an average spine density across the cortex. Lastly, specific to dendritic length, we used data using intracellular dye injections (biocytin) and then mapped in 3D space using Neurolucida software (Mohan et al. 2015) rather than data based on the rapid Golgi stain protocol (Bianchi et al. 2012, 2013).

The use of surface area in this report may be indirectly capturing the amount of bound protons, or the amount of macromolecular docking/hydration sites that facilitate efficient exchange (Ceckler et al. 1992; Koenig et al. 1993; Koenig 1996). For simplicity's sake, we ignore the effect of myelin water and focus on the surface area by which maximal transfer (spin diffusion) can occur. We speculate that the effect of myelin water, the water found between the inner layers of myelin, is minimal because only 2–3% of all protons are associated with myelin water in the cerebral cortex (Vavasour et al. 1998). Although myelin possesses a higher saturation exchange rate than axon/cellular membrane, its greater longitudinal relaxation rate results in comparable MTR values to axonal membranes in peripheral nerve of the African clawed toad (Does et al. 1998). Myelinated and nonmyelinated nerves have similar MTR values, suggesting that cellular membranes and myelin contribute similarly to MTR, regardless of their very different molecular composition (Beaulieu 1994). To err on the side of caution, even if we consider the effect of myelin water in MT, it would not be as large as the effect of a 34-fold increase in surface area due to dendrites (and their spines). This is validated by a model of hypomyelinated pups that have minimal change in the bound-proton pool fraction size in whole cortical gray matter, and present only a 7% decrease in MTR of the caudate nucleus (subcortical gray matter) compared with controls (Samsonov et al. 2012). The rather small reduction of MTR in a hypomyelinated model suggests that myelin is not the biggest contributor to MTR signal, concurrent with our findings on absolute MTR.

Limitations

One of the limitations of the current analysis is the scarcity of gene expression data, both in terms of number of donors and their age range. To some extent, this is mitigated by a 2-stage validation procedure that includes a comparison of the Allen Human Brain Atlas with an independent dataset (BrainSpan). Age-related increases in cortical MT reported by Whitaker et al. (2016) are replicated in this cohort using an MTR sequence. We do not replicate, however, the negative relationship between MT and cortical thickness across the cortex (Whitaker et al. 2016). This may be due to differences in the MRI sequence,

namely, MTR used in our study versus semiquantitative MT used by Whitaker et al. (2016). In particular, Whitaker et al. employed a multiecho acquisition sequence and acquired images with 1-mm isotropic resolution, compared with 0.875 × 0.875 × 3.0 mm^3 used in this study. The off-resonance radiofrequency pulse used by Whitaker et al. was at 2000 Hz, while we used a 1000 Hz pulse. Generally speaking, it is difficult to compare MTR (or semiquantitative MT) studies across different centers and with different acquisition parameters (Tofts 2003). Note, however, that MTR profiles obtained on the same scanner 4 years apart (i.e., at Visits 1 and 2) are highly reproducible. Future histological studies demonstrating the relationship between MTR and dendritic arbor are warranted to confirm findings from virtual histology.

Conclusion

In summary, we observe an increase in mean MTR values in the human cerebral cortex with age during adolescence in both sexes. Inter-regional variation in absolute MTR at a single timepoint is driven by macromolecules associated with cellular membranes of dendritic arbor, whereas the inter-regional profile in ΔMTR appears to be driven by intracortical myelination.

Supplementary Material

Supplementary material is available at *Cerebral Cortex* online.

Author Contributions

Y.P. analyzed the data. S.J. designed statistical analysis between cell-specific gene expression and MRI-metrics. Y.P., S.J., P.A.G., Z.P., and T.P. contributed to writing and editing of the article. P. A.G. designed the MTR sequence. Z.P. and T.P. were involved in the IMAGEN study design. T.P. and P.A.G. are current members of the IMAGEN consortium.

Notes

We thank Dr Christiaan P.J. de Kock and collaborators from Mohan et al. (2015) for assistance with metrics of dendritic arbour in order to construct a model of membranes. Additionally, we would like to thank Dr Hermann Cuntz and collaborators from Cuntz et al. (2010) for providing a neuronal construction (Fig. 1). *Conflict of Interest*: None declared.

Funding

This work received support from the following sources: the European Union-funded FP6 Integrated Project IMAGEN (Reinforcement-related behaviour in normal brain function and psychopathology) (LSHM-CT- 2007-037286), the Horizon 2020 funded ERC Advanced Grant 'STRATIFY' (Brain network based stratification of reinforcement-related disorders) (695313), ERANID (Understanding the Interplay between Cultural, Biological and Subjective Factors in Drug Use Pathways) (PR-ST-0416-10004), BRIDGET (JPND: BRain Imaging, cognition Dementia and next generation GEnomics) (MR/N027558/1), the FP7 projects IMAGEMEND(602450; IMAging GEnetics for MENtal Disorders) and MATRICS (603016), the Innovative Medicine Initiative Project EU-AIMS (115300-2), the Medical Research Council Grant 'c-VEDA' (Consortium on Vulnerability to Externalizing Disorders and Addictions) (MR/N000390/1), the Swedish Research Council FORMAS, the Medical Research Council, the National Institute for Health Research (NIHR) Biomedical Research Centre at South London and Maudsley NHS Foundation Trust and King's College London, the Bundesministeriumfür Bildung und Forschung (BMBF grants 01GS08152; 01EV0711; eMED SysAlc01ZX1311A; Forschungsnetz AERIAL), the Deutsche Forschungsgemeinschaft (DFG grants SM 80/7-1, SM 80/7-2, SFB 940/1). Further support was provided by grants from: ANR (project AF12-NEUR0008-01 - WM2NA, and ANR-12-SAMA-0004), the Fondation de France, the Fondation pour la Recherche Médicale, the Mission Interministérielle de Lutte-contre-les-Drogues-et-les-Conduites-Addictives (MILDECA), the Assistance-Publique-Hôpitaux-de-Paris and INSERM (interface grant), Paris Sud University IDEX 2012; the National Institutes of Health, Science Foundation Ireland (16/ERCD/3797), U.S.A. (Axon, Testosterone and Mental Health during Adolescence; RO1 MH085772-01A1), and by NIH Consortium grant U54 EB020403, supported by a cross-NIH alliance that funds Big Data to Knowledge Centres of Excellence.

References

Azevedo FA, Carvalho LR, Grinberg LT, Farfel JM, Ferretti RE, Leite RE, Lent R, Herculano-Houzel S. 2009. Equal numbers of neuronal and nonneuronal cells make the human brain an isometrically scaled-up primate brain. J Comp Neurol. 513:532–541.

Beaulieu C. 1994. Some magnetisation transfer properties of water in myelinated and nonmyelinated nerves. Book Abstr Second Annu Meet Soc Magn Reson. 169.

Belton P, Hills B, Raimbaud E. 1988. The effects of morphology and exchange on proton NMR relaxation in agarose gels. Mol Phys. 63:825–842.

Benavides-Piccione R, Ballesteros-Yáñez I, DeFelipe J, Yuste R. 2002. Cortical area and species differences in dendritic spine morphology. J Neurocytol. 31:337–346.

Benavides-Piccione R, Fernaud-Espinosa I, Robles V, Yuste R, DeFelipe J. 2012. Age-based comparison of human dendritic spine structure using complete three-dimensional reconstructions. Cereb Cortex. 23:1798–1810.

Benes FM, Turtle M, Khan Y, Farol P. 1994. Myelination of a key relay zone in the hippocampal formation occurs in the human brain during childhood, adolescence, and adulthood. Arch Gen Psychiatry. 51:477–484.

Bianchi S, Stimpson CD, Bauernfeind AL, Schapiro SJ, Baze WB, McArthur MJ, Bronson E, Hopkins WD, Semendeferi K, Jacobs B. 2012. Dendritic morphology of pyramidal neurons in the chimpanzee neocortex: regional specializations and comparison to humans. Cereb Cortex. 23:2429–2436.

Bianchi S, Stimpson CD, Duka T, Larsen MD, Janssen WG, Collins Z, Bauernfeind AL, Schapiro SJ, Baze WB, McArthur MJ. 2013. Synaptogenesis and development of pyramidal neuron dendritic morphology in the chimpanzee neocortex resembles humans. Proc Natl Acad Sci USA. 110:10395–10401.

Carlson M. 2016a. A set of annotation maps describing the entire Gene Ontology. R package.

Carlson M. 2016b. org.Hs.eg.db: Genome wide annotation for Human. R package.

Ceckler TL, Wolff SD, Yip V, Simon SA, Balaban RS. 1992. Dynamic and chemical factors affecting water proton relaxation by macromolecules. J Magn Reson. 98:637–645.

Cuntz H, Forstner F, Borst A, Häusser M. 2010. One rule to grow them all: a general theory of neuronal branching and its practical application. PLoS Comput Biol. 6:e1000877.

Dale AM, Fischl B, Sereno MI. 1999. Cortical surface-based analysis: I. Segmentation and surface reconstruction. Neuroimage. 9:179–194.

De Boer RW. 1995. Magnetization transfer contrast. Part 1: MR Physics. Philips Med Syst. 40:64–73.
DeFelipe J. 2011. The evolution of the brain, the human nature of cortical circuits, and intellectual creativity. Front Neuroanat. 5:29.
DeFelipe J, Fariñas I. 1992. The pyramidal neuron of the cerebral cortex: morphological and chemical characteristics of the synaptic inputs. Prog Neurobiol. 39:563–607.
Desikan RS, Ségonne F, Fischl B, Quinn BT, Dickerson BC, Blacker D, Buckner RL, Dale AM, Maguire RP, Hyman BT. 2006. An automated labeling system for subdividing the human cerebral cortex on MRI scans into gyral based regions of interest. Neuroimage. 31:968–980.
Does MD, Beaulieu C, Allen PS, Snyder RE. 1998. Multicomponent T 1 relaxation and magnetisation transfer in peripheral nerve. Magn Reson Imaging. 16:1033–1041.
Edzes HT, Samulski ET. 1977. Cross relaxation and spin diffusion in the proton NMR of hydrated collagen. Nature. 265:521.
Elston GN, Benavides-Piccione R, DeFelipe J. 2001. The pyramidal cell in cognition: a comparative study in human and monkey. J Neurosci. 21:RC163–168.
Eyal G, Verhoog MB, Testa-Silva G, Deitcher Y, Lodder JC, Benavides-Piccione R, Morales J, DeFelipe J, de Kock CP, Mansvelder HD. 2016. Unique membrane properties and enhanced signal processing in human neocortical neurons. Elife.. 5:e16553.
Filippi M, Rocca MA, Martino G, Horsfield MA, Comi G. 1998. Magnetization transfer changes in the normal appering white matter precede the appearance of enhancing lesions in patients with multiple sclerosis. Ann Neurol. 43: 809–814.
Fjær S, Bø L, Lundervold A, Myhr K-M, Pavlin T, Torkildsen Ø, Wergeland S. 2013. Deep gray matter demyelination detected by magnetization transfer ratio in the cuprizone model. PLoS One. 8:e84162.
French L, Paus T. 2015. A FreeSurfer view of the cortical transcriptome generated from the Allen Human Brain Atlas. Front Neurosci. 9:323.
Gibson EM, Purger D, Mount CW, Goldstein AK, Lin GL, Wood LS, Inema I, Miller SE, Bieri G, Zuchero JB. 2014. Neuronal activity promotes oligodendrogenesis and adaptive myelination in the mammalian brain. Science. 344:1252304.
Glasser MF, Sotiropoulos SN, Wilson JA, Coalson TS, Fischl B, Andersson JL, Xu J, Jbabdi S, Webster M, Polimeni JR. 2013. The minimal preprocessing pipelines for the Human Connectome Project. Neuroimage. 80:105–124.
Greve DN, Fischl B. 2009. Accurate and robust brain image alignment using boundary-based registration. Neuroimage. 48:63–72.
Grossman RI, Gomori JM, Ramer KN, Lexa FJ, Schnall MD. 1994. Magnetization transfer: theory and clinical applications in neuroradiology. Radiographics. 14:279–290.
Guadiana SM, Semple-Rowland S, Daroszewski D, Madorsky I, Breunig JJ, Mykytyn K, Sarkisian MR. 2013. Arborization of dendrites by developing neocortical neurons is dependent on primary cilia and type 3 adenylyl cyclase. J Neurosci. 33: 2626–2638.
Gyllensten L, Malmfors T. 1963. Myelinization of the optic nerve and its dependence on visual function—a quantitative investigation in mice. Development. 11:255–266.
Hawrylycz MJ, Lein ES, Guillozet-Bongaarts AL, Shen EH, Ng L, Miller JA, Van De Lagemaat LN, Smith KA, Ebbert A, Riley ZL. 2012. An anatomically comprehensive atlas of the adult human brain transcriptome. Nature. 489:391.
Henkelman RM, Huang X, Xiang Q, Stanisz G, Swanson SD, Bronskill MJ. 1993. Quantitative interpretation of magnetization transfer. Magn Reson Med. 29:759–766.
Henkelman R, Stanisz G, Graham S. 2001. Magnetization transfer in MRI: a review. NMR Biomed. 14:57–64.
Huttenlocher PR, De Courten C. 1987. The development of synapses in striate cortex of man. Hum Neurobiol. 6:1–9.
Innocenti GM, Vercelli A, Caminiti R. 2013. The diameter of cortical axons depends both on the area of origin and target. Cereb Cortex. 24:2178–2188.
Ishikawa H, Thompson J, Yates JR, Marshall WF. 2012. Proteomic analysis of mammalian primary cilia. Curr Biol. 22:414–419.
Jensen SK, Yong VW. 2016. Activity-dependent and experience-driven myelination provide new directions for the management of multiple sclerosis. Trends Neurosci. 39:356–365.
Koenig SH. 1996. Molecular basis of magnetic relaxation of water protons of tissue. Acad Radiol. 3:597–606.
Koenig SH, Brown RD III, Ugolini R. 1993. Magnetization transfer in cross-linked bovine serum albumin solutions at 200 MHz: a model for tissue. Magn Reson Med. 29:311–316.
Lebel C, Beaulieu C. 2011. Longitudinal development of human brain wiring continues from childhood into adulthood. J Neurosci. 31:10937–10947.
Lee JH, Gleeson JG. 2010. The role of primary cilia in neuronal function. Neurobiol Dis. 38:167–172.
Lerch JP, van der Kouwe AJ, Raznahan A, Paus T, Johansen-Berg H, Miller KL, Smith SM, Fischl B, Sotiropoulos SN. 2017. Studying neuroanatomy using MRI. Nat Neurosci. 20:314.
Liewald D, Miller R, Logothetis N, Wagner H-J, Schüz A. 2014. Distribution of axon diameters in cortical white matter: an electron-microscopic study on three human brains and a macaque. Biol Cybern. 108:541–557.
Luo W. 2009. Spin diffusion and dynamics studies of the channel forming membrane proteins by solid-state nuclear magnetic resonance. Iowa State University.
Mangeat G, Govindarajan ST, Mainero C, Cohen-Adad J. 2015. Multivariate combination of magnetization transfer, T 2* and B0 orientation to study the myelo-architecture of the in vivo human cortex. Neuroimage. 119:89–102.
Markram H, Toledo-Rodriguez M, Wang Y, Gupta A, Silberberg G, Wu C. 2004. Interneurons of the neocortical inhibitory system. Nat Rev Neurosci. 5:793–807.
Miller DJ, Duka T, Stimpson CD, Schapiro SJ, Baze WB, McArthur MJ, Fobbs AJ, Sousa AM, Šestan N, Wildman DE. 2012. Prolonged myelination in human neocortical evolution. Proc Natl Acad Sci USA. 109:16480–16485.
Mohan H, Verhoog MB, Doreswamy KK, Eyal G, Aardse R, Lodder BN, Goriounova NA, Asamoah B, B Brakspear AB, Groot C, et al. 2015. Dendritic and axonal architecture of individual pyramidal neurons across layers of adult human neocortex. Cereb Cortex. 25:4839–4853.
Nawaz S, Kippert A, Saab AS, Werner HB, Lang T, Nave K-A, Simons M. 2009. Phosphatidylinositol 4, 5-bisphosphate-dependent interaction of myelin basic protein with the plasma membrane in oligodendroglial cells and its rapid perturbation by elevated calcium. J Neurosci. 29:4794–4807.
Pakkenberg B, Gundersen HJG. 1997. Neocortical neuron number in humans: effect of sex and age. J Comp Neurol. 384: 312–320.
Pazour GJ, Witman GB. 2003. The vertebrate primary cilium is a sensory organelle. Curr Opin Cell Biol. 15:105–110.
Petanjek Z, Judaš M, Šimić G, Rašin MR, Uylings HB, Rakic P, Kostović I. 2011. Extraordinary neoteny of synaptic spines in

the human prefrontal cortex. Proc Natl Acad Sci USA. 108: 13281–13286.

Rakic P, Bourgeois J-P, Goldman-Rakic P. 1994. Synaptic development of the cerebral cortex: implications for learning, memory, and mental illness. Prog Brain Res. 102:227–243.

Sala C, Segal M. 2014. Dendritic spines: the locus of structural and functional plasticity. Physiol Rev. 94:141–188.

Samsonov A, Alexander AL, Mossahebi P, Wu Y-C, Duncan ID, Field AS. 2012. Quantitative MR imaging of two-pool magnetization transfer model parameters in myelin mutant shaking pup. Neuroimage. 62:1390–1398.

Schmierer K, Scaravilli F, Altmann DR, Barker GJ, Miller DH. 2004. Magnetization transfer ratio and myelin in postmortem multiple sclerosis brain. Ann Neurol. 56:407–415.

Schumann G, Loth E, Banaschewski T, Barbot A, Barker G, Büchel C, Conrod P, Dalley J, Flor H, Gallinat J. 2010. The IMAGEN study: reinforcement-related behaviour in normal brain function and psychopathology. Mol Psychiatry. 15:1128.

Seiler S, Ropele S, Schmidt R. 2014. Magnetization transfer imaging for in vivo detection of microstructural tissue changes in aging and dementia: a short literature review. J Alzheimers Dis. 42:S229–S237.

Shin J, French L, Xu T, Leonard G, Perron M, Pike GB, Richer L, Veillette S, Pausova Z, Paus T. 2017. Cell-specific gene-expression profiles and cortical thickness in the human brain. Cereb Cortex. 1–11.

Tamnes CK, Herting MM, Goddings A-L, Meuwese R, Blakemore S-J, Dahl RE, Güroğlu B, Raznahan A, Sowell ER, Crone EA. 2017. Development of the cerebral cortex across adolescence: a multisample study of inter-related longitudinal changes in cortical volume, surface area, and thickness. J Neurosci. 37:3402–3412.

Tofts P. 2003. Quantitative MRI of the brain: measuring changes caused by disease. Chichester, West Sussex; Hoboken, NJ: Wiley.

Trapp BD, Kidd GJ. 2004. Structure of the myelinated axon. In: Robert AL, John WG, Hans L, Klaus-Armin N, Robert M, Bruce DT, editors. Myelin biology and disorders. Cleveland, OH: Elsevier. p. 3–27.

Ulfhake B, Kellerth J. 1981. A quantitative light microscopic study of the dendrites of cat spinal α-motoneurons after intracellular staining with horseradish peroxidase. J Comp Neurol. 202:571–583.

Vavasour IM, Whittall KP, Mackay AL, Li DK, Vorobeychik G, Paty DW. 1998. A comparison between magnetization transfer ratios and myelin water percentages in normals and multiple sclerosis patients. Magn Reson Med. 40:763–768.

Weiner J 3rd, Domaszewska T. 2016. tmod: an R package for general and multivariate enrichment analysis. PeerJ Prepr.

Whitaker KJ, Vértes PE, Romero-Garcia R, Váša F, Moutoussis M, Prabhu G, Weiskopf N, Callaghan MF, Wagstyl K, Rittman T, et al. 2016. Adolescence is associated with genomically patterned consolidation of the hubs of the human brain connectome. Proc Natl Acad Sci USA. 113:9105–9110.

Wong AP-Y, French L, Leonard G, Perron M, Pike GB, Richer L, Veillette S, Pausova Z, Paus T. 2017. Inter-regional variations in gene expression and age-related cortical thinning in the adolescent brain. Cereb Cortex. 28:1–10.

Zeisel A, Muñoz-Manchado AB, Codeluppi S, Lönnerberg P, La Manno G, Juréus A, Marques S, Munguba H, He L, Betsholtz C. 2015. Cell types in the mouse cortex and hippocampus revealed by single-cell RNA-seq. Science. 347: 1138–1142.